Hindawi
Science and Technology of Nuclear Installations
Volume 2022, Article ID 3544436, 16 pages
https://doi.org/10.1155/2022/3544436

Research Article

Influence of Weak Compressibility on the Hydrodynamic Performance Evaluation of Pump Turbines in the Pump Mode

Fangfang Zhang,[1,2] **Na Li**,[3] **Di Zhu**,[4] **Ruofu Xiao**,[1,2] **Weichao Liu**,[5] **and Ran Tao**[1,2]

[1]*College of Water Resources and Civil Engineering, China Agricultural University, Beijing 100083, China*
[2]*Beijing Engineering Research Center of Safety and Energy Saving Technology for Water Supply Network System, China Agricultural University, Beijing 100083, China*
[3]*China Irrigation and Drainage Development Center, Beijing 100000, China*
[4]*College of Engineering, China Agricultural University, Beijing 100083, China*
[5]*Dongfang Electric Machinery Co. Ltd., Deyang 618000, China*

Correspondence should be addressed to Ran Tao; randytao@cau.edu.cn

Received 22 February 2022; Accepted 3 May 2022; Published 20 May 2022

Academic Editor: Iztok Tiselj

In general, weak compressibility is one of the properties of liquids. That is, in actual operation of hydraulic machinery, the flow is weakly compressible. However, the influence of weak compressibility is often neglected in usual numerical simulation, which makes the simulation results different from the experimental results. Based on the Computational Fluid Dynamics (CFD) solver and model test rig, by means of mutual verification between numerical simulation and experiment, the fitting degree between numerical results and experimental results before and after considering weak compressibility is compared and analyzed in this paper; it is obtained that the numerical results is closer to the experimental results after considering the weak compressibility. In addition, velocity field of pump turbines, head loss of main components, and the change of entropy yield are analyzed and reasons for numerical value being closer to the experimental value after considering weak compressibility of fluid are summarized and analyzed. It is proved that the consideration of weak compressibility is of great significance to improve the accuracy of results in the numerical simulation of pump turbines.

1. Introduction

With the continuous development of nuclear power technology, the construction of nuclear power plants around the world is gradually increasing. The operation cost of nuclear power is low, but variable load is difficult and accompanied by huge technical risks, so it is not suitable for peak shaving [1]. At present, the construction of pumped storage power station as a supporting equipment of nuclear power for peak shaving has become popular [2, 3]. There are currently many popular energy storage techniques including electrochemical energy storage, electromagnetic energy storage, and mechanical energy storage [4–6]. Among them, pumped storage technology which is a kind of mechanical energy storage has the advantages of large capacity, strong stability, and flexible start and stop [7]. It can also play the roles of phase modulation, frequency modulation, load tracking, and accident standby in the power system. Therefore, pumped storage technology has become one of the best choices to cooperate with nuclear power plants [8].

The reversible pump turbine is the key component in pumped storage hydropower stations [9]. It consumes electric energy through drawing water to a high place in the pump mode and electric energy is transformed into mechanical energy and then into potential energy of water in the process, so as to achieve the purpose of energy storage. When the electric energy needs to be utilized, the power generation is carried out in turbine mode to convert the potential energy in the water into mechanical energy, so as to generate electric power; it makes the pump turbine play an important role in the whole process of energy storage [10, 11]. During the operation of pump turbines in the pump

mode, the head, efficiency, and power are often monitored as key parameters [12, 13]; numerical simulation based on Computational Fluid Dynamics (CFD) is used as a common means to analyze the internal flow field of the whole turbomachinery and predict the hydrodynamic performances [14, 15]. However, during the process of numerical simulation, it is usually assumed that the flow is incompressible and then time homogenization is carried out to obtain Reynolds equation as the simulation basics, but the method of using inviscid flow to approximate Reynolds flow is not suitable to describe the condition that flow closely related to time [16–18]. In fact, the actual flow in hydraulic machinery is weakly compressible, the weakly compressible flow refers to the flow with little change in fluid density; that is, the flow is a low Mach number flow [19]. Most liquids have this characteristic, so considering the compressibility of the fluid can make the calculation results more reasonable [20, 21].

Since Song et al. [22] proposed a weakly compressible flow model in 1988, scholars have conducted rich research results on one-dimensional pipeline and three-dimensional solid based on the model. Martins et al. [23] used the weakly compressible model to simulate the hydraulic transient flow in the pressure pipe and analyzed the pressure wave propagation and velocity distribution. Based on the one-dimensional friction model and three-dimensional turbulence model and the weakly compressible flow model, Wu et al. [24] combined the pressure-density model with the three-dimensional continuity equation to study the transient flow characteristics and dissipation mechanism in the pressure pipe. Tang et al. [25] studied the transient noncavitating flow and cavitating flow caused by closing the valve quickly in the reservoir pipe valve system based on the weakly compressible model and verified the reliability of RANS method for weakly compressible fluid through experiments.

Based on the previous studies and theories, aiming at a pump turbine subject, the influence of flow compressibility on its energy performance in the pump mode will be carried out. Focusing on the adjustable guide vane part with the strongest response to flow weak compressibility, and the flow pattern character under different guide vane openings will be analyzed; the study is of great significance to the efficient and stable operation for pump turbine units.

2. Numerical Method

2.1. Governing Equations. Combining with the weakly compressible flow model proposed by Song et al. [22], based on the laws of conservation of mass and conservation of momentum, the continuity equation and momentum equation for compressible fluid can be expressed by

$$\frac{\partial \rho}{\partial t} + \nabla \cdot (\rho u) = 0, \tag{1}$$

$$\frac{\partial u}{\partial t} + u \cdot \nabla u + \nabla \frac{p}{\rho} = 0, \tag{2}$$

where ρ is the density of the liquid, here water in 25°C, $\rho = 999.8\ \mathrm{kg/m^3}$, t is the time, u is velocity, and p is the pressure.

The propagation speed of sound in water can be expressed by

$$a^2 = \frac{\partial p}{\partial \rho}. \tag{3}$$

For barotropic flow, the pressure at every point in the fluid domain is only related to density of fluid. Substituting equation (3) into equations (1) and (2), the continuity equation and momentum equation for barotropic flow can be obtained and expressed by following formulas:

$$\frac{\partial p}{\partial t} + \rho a^2 \nabla \cdot u + u \cdot \nabla p = 0, \tag{4}$$

$$\frac{\partial u}{\partial t} + u \cdot \Delta u + \nabla \frac{p}{\rho} + \frac{p}{\rho^2 a^2} \Delta p = 0. \tag{5}$$

When analyzing the dimensional parameters, in order to establish the equation and facilitate the operation, the dimensionless parameters are carried out based on Strouhal Number principle. Therefore, in order to standardize the expression, the dimensionless parameters in equations (4) and (5) can be obtained:

$$\begin{aligned} SM^2\left(\frac{\partial p^*}{\partial t^*}\right) + \rho^* \nabla^* \cdot u^* + M^2 u^* \cdot \nabla^* p^* &= 0, \\ S\frac{\partial u^*}{\partial t^*} + (u^* \cdot \nabla^*) u^* + \nabla^* \frac{p^*}{\rho^*} + M^2 \frac{p^*}{(\rho^* a^*)^2} \nabla^* p^* &= 0, \end{aligned} \tag{6}$$

where the asterisk represents the dimensionless parameters, $\rho^* = \rho/\rho_0$, $t^* = t/t_0$, $u^* = u/u_0$, $p^* = (p - p_\infty)/\rho_0 u_0^2$, u_0 is the reference velocity, t_0 is the reference time, and l_0 is the reference length; $S = l_0/t_0 u_0$ represents Strouhal Number, and $M = u_0/a_0$ represents Mach Number.

For weakly compressible flow, the value of Mach number is very small, a can be regarded as a constant number. Therefore, the governing equations of weakly compressible flow can be simplified into

$$\begin{aligned} \frac{\partial p}{\partial t} + E \nabla \cdot u &= 0, \\ \frac{\partial u}{\partial t} + u(\nabla \cdot u) + \nabla \frac{p}{\rho} &= 0, \end{aligned} \tag{7}$$

where $E = \rho a^2$ is bulk modulus.

2.2. Turbulence Model. In the process of numerical simulation based on computational fluid dynamics, the choice of turbulence model is very important. The SST k-ω turbulence model has the following advantages: (a) SST k-ω model considers the transmission of turbulent shear stress, while the model can predict the beginning of the flow and the flow separation under negative pressure gradient. (b) SST k-ω model has high calculation accuracy for free shear turbulence, turbulence attached with boundary layer, and moderately separated turbulence. (c) SST k-ω turbulence model has high inclusiveness [26]. (d) Compared with other turbulence models, SST k-ω turbulence model not only

enhances the wall function but also avoids the problem that the grids near the wall are over dense, and it makes the computing result not too sensitive to the wall grids, and the whole solution process has high stability and accuracy. Therefore, SST k-ω model is selected as the turbulence prediction model in this study.

The turbulent kinetic energy equation and the transport equation of specific turbulence dissipation rate equation of SST k-ω model can be expressed as

$$\frac{\partial}{\partial t}(\rho k) + \frac{\partial}{\partial x_i}(\rho k u_i) = \frac{\partial}{\partial x_j}\left(\Gamma_k \frac{\partial k}{\partial x_j}\right) + G_k - Y_k + S_K,$$

$$\frac{\partial}{\partial t}(\rho \omega) + \frac{\partial}{\partial x_i}(\rho \omega u_i) = \frac{\partial}{\partial x_j}\left(\Gamma_\omega \frac{\partial \omega}{\partial x_j}\right) + G_\omega - Y_\omega + D_\omega + S_\omega, \tag{8}$$

where k is turbulent kinetic energy, ω is the turbulence dissipation rate, Γ_k is the effective diffusion term of k, Γ_ω is the effective diffusion term of ω, G_k is the kinetic energy of turbulence, D_ω is orthogonal divergent term, Y_k is the divergent term of k, and Y_ω is divergent term of ω.

2.3. Weak Compressibility. In general, fluid is regarded as incompressible medium. However, in the actual operation process of hydraulic machinery, the speed of water flow u usually exceeds 1 m/s, but it is also smaller than the propagation speed of sound wave in water $a = 1000$ m/s; that is, u is always greater than 1 m/s and far less than the propagation speed of sound wave in water $a = 1000$ m/s. According to the expression of Mach number, $M = u/a$ and the liquid in hydraulic machinery meets low Mach number flow, which proves the liquid in hydraulic machinery has weak compressibility. Therefore, the weak compressibility of the fluid should be considered in the process of numerical simulation, and it will make the simulation process closer to the real flow.

When considering the weak compressibility of fluid, the fluid density is no longer a constant number, but a function of pressure, and it changes with the change of pressure. The expression is as follows:

$$\rho = \rho_0 \times \left(1 + \frac{p - p_0}{E}\right), \tag{9}$$

where ρ_0 is a constant number, here, $\rho_0 = 1002\,\text{kg/m}^3$, p is pressure, p_0 is the known reference pressure, E is the bulk modulus of water, and its value is 2.2×10^9 Pa. As it can be seen in equation (9), when the pressure increases, the liquid is compressed, the volume of the liquid decreases, and the mass remains unchanged, and so the density increases. That is to say, a 0.1% change in density requires the application of 22 atmospheres.

3. CFD Simulation

3.1. Preprocessing. Numerical simulation is used in this study to analyze the internal flow field details. Commercial software CFX is used in this study for the flow in the objective pump turbine. As shown in Figure 1(a), the fluid domain of the whole pump turbine is composed of suction chamber (when in the turbine mode, it is called draft tube), impeller, guide vane, stay vane, volute, and extended tube section. In the pump mode, the water flows from the suction chamber through impeller, guide vane, and stay vane and finally through volute out to the extended tube section. The rotation speed of impeller n_d is 1200 r/min, the design flow rate Q_d is 450 kg/s, and the design head H_d is 54 m. The specific speed is an important parameter reflecting the performance of rotating hydraulic machinery. Under the pump mode, for the objective pump turbine researched in this study, the specific speed n_s can be expressed as follows:

$$n_s = \frac{n_d \sqrt{Q_d}}{H_d^{3/4}}. \tag{10}$$

In this case, the value of specific speed is approximately 40.41. The axial projection draw of impeller is shown in Figure 1(b), while its geometric parameters are shown in Table 1.

In the whole fluid domain, the flow medium is water and the reference pressure is 1 atm. In the process of CFD pretreatment settings, the inlet of the suction chamber in the pump mode is used as the inlet of the whole fluid domain and the outlet of the extended tube section is used as the outlet of the whole fluid domain. The inlet is set as the flow boundary, and the flow value changes with different simulation conditions; the outlet is set as the pressure boundary. In the whole pump turbine, the impeller rotates at the speed of 1200 r/min and the rest components are all stationary; the opening of guide vane is adjusted by the hydraulic controlled system. In this study, the adjustment values of the opening of the guide vane are 10°, 12°, and 14°. Set all the walls in fluid domain as no slip walls. In order to realize the transmission of calculated values between every two flow-through components, the settings of interface are of great importance. Therefore, a static-static interface is set between each two stationary parts, such as the interface between guide vane and stay vane, stay vane and volute, volute and extension tube section; the dynamic-static interface is set between the stationary components and the rotating components, such as the interface between the suction chamber and the impeller and the interface between the impeller and the guide vane.

The fluid domain is discretized for CFD simulation. As shown in Figure 2, it is the division situation of the whole fluid-domain grid, the commercial software ICEM CFD is used for every component of fluid domain, in which the suction chamber, impeller, guide vane, stay vane, and extension tube section are structure grid with hexahedral elements, while the volute is unstructured grid with tetrahedral elements. In order to ensure the convergence of the wall function in the solving process, the boundary layer grid of each component is encrypted to make the y^+ value on the wall boundary between 30 and 300. In the whole solving process, the maximum number of iterative steps is set to 600 and the convergence criterion of momentum equation and

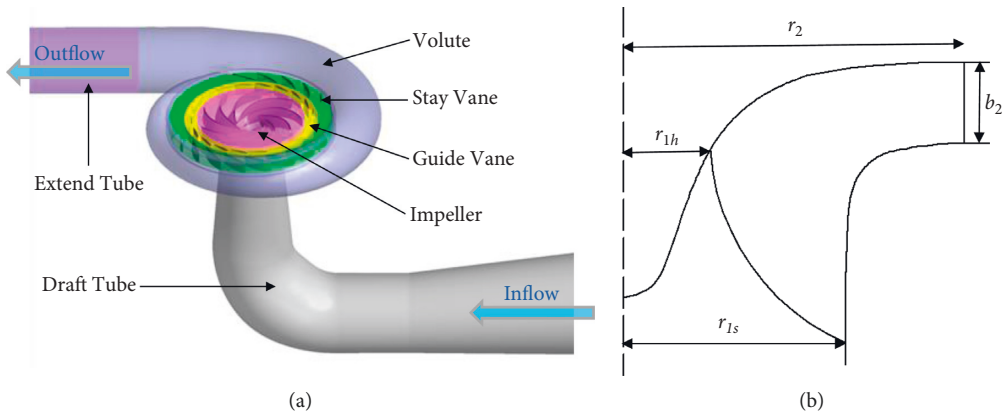

Figure 1: Objective pump turbine model. (a) Fluid domain schematic. (b) Meridian shape of the impellent.

Table 1: Geometric parameters of the objective pump turbine.

Parameters	Values	Unit
Impeller radius of leading edge at shroud side r_{1s}	150	(Mm)
Impeller radius of leading edge at hub side r_{1h}	70	(Mm)
Impeller radius of trailing edge r_2	257	(Mm)
Impeller width at outlet b_2	570	(Mm)
Impeller blade number Z_1	9	(—)
Guide vane blade number Z_2	20	(—)
Stay vane blade number Z_3	20	(—)

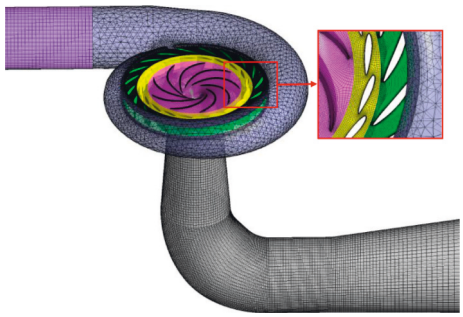

Figure 2: Schematic of the grid of the fluid domain.

continuity equation is 0.00001. In this study, based on the above settings, the head, efficiency, and power of the pump turbine under different openings are monitored. Based on these, the influence of weak compressibility of fluid on the pump turbine is studied.

3.2. Grid Independence Check. As for the verification of grid independence, in order to avoid the complexity of conventional methods to analyze the trend of a specific parameter with the growth of the grid number, this study uses the grid convergence index (GCI) method based on Richardson extrapolation to judge the convergence of the grid [27, 28]. In this extrapolation method, three sets of grid independence checks are carried out for the three kinds of guide vane openings studied in this paper. The details are shown in Figure 3. Under every opening, the grid number for fine, medium, and coarse schemes are shown in Table 2. Under the three objective openings of guide vane, the refinement factor of adjacent grids is greater than 1.3, and the convergence index of fine grid and coarse grid is less than 5%, which meets the convergence requirements. Therefore, the grid independence is verified.

Because the nine grid schemes of three objective guide vane openings used for the grid independence check all meet the convergence requirements, it is feasible to select any set of grids above. Considering the actual computing resources and the grid convergence index, the grid number of coarse grid scheme is only relatively small but also is a number of million orders. Therefore, the coarse grid scheme N3 is selected as the final grid scheme used to simulation.

4. Model Test of Performance

Figure 4 is the schematic diagram of the test rig used in this study. Based on this test rig, the energy parameters of the objective pump turbine in pump mode can be obtained, including flow rate, rotation speed, torque, shaft power, head, and efficiency. The measurement is based on the IEC 60193 standard [29]. The test rig is divided into two main lines: fluid transmission chain and information transmission chain. One is the flow direction of the fluid inside the pump turbine in pump mode, and the other is the information chain of data transmission.

In the model test, the electromagnetic flowmeter is used to monitor the flow rate Q in the pipeline and the errors of the instruments are less than ±2%. The rotation speed of impeller n is measured by using the encoder which is connected to the shaft of generator; the main torque M is measured by the dynamometer motor and load sensors, and the error of the instruments are less than ±0.1%; head H is the total pressure difference of the inlet and outlet of the pump turbine in the pump mode. The static pressure difference of the inlet and outlet is measured by the differential pressure sensors, and the error of the differential pressure sensors is no more than ±0.1%, while the dynamic head is obtained by integrating the test flow rate and the sectional area for pressure measurement of inlet and outlet.

Based on the measured values of the above test rig instruments, the head H is calculated by

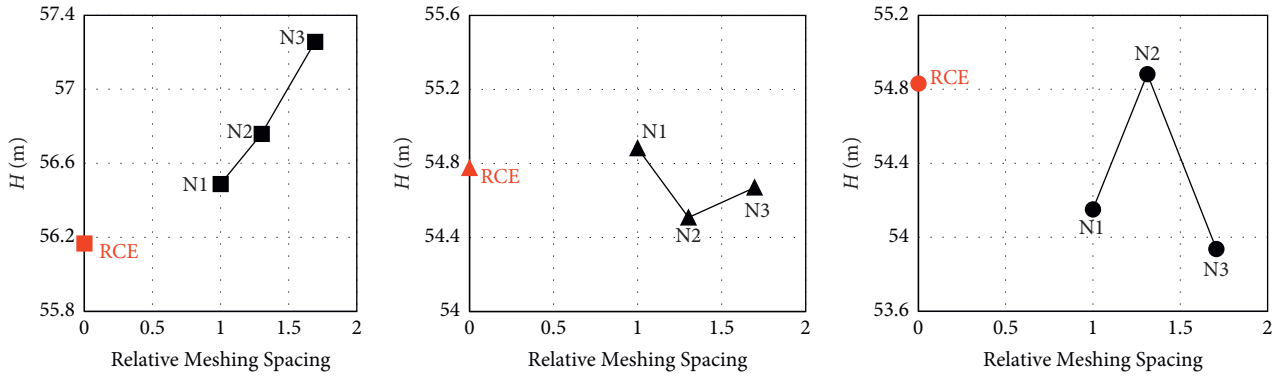

Figure 3: Grid independent check for three specific guide vane degrees based on GCI. RCE: Richardson extrapolated value.

Table 2: Node number of different grid schemes.

Schemes	$\alpha = 10$ deg	$\alpha = 12$ deg	$\alpha = 14$ deg
N1 (fine)	12200607	12650696	12883899
N2 (medium)	5542979	5726859	5840087
N3 (coarse)	2509940	2590900	2589380

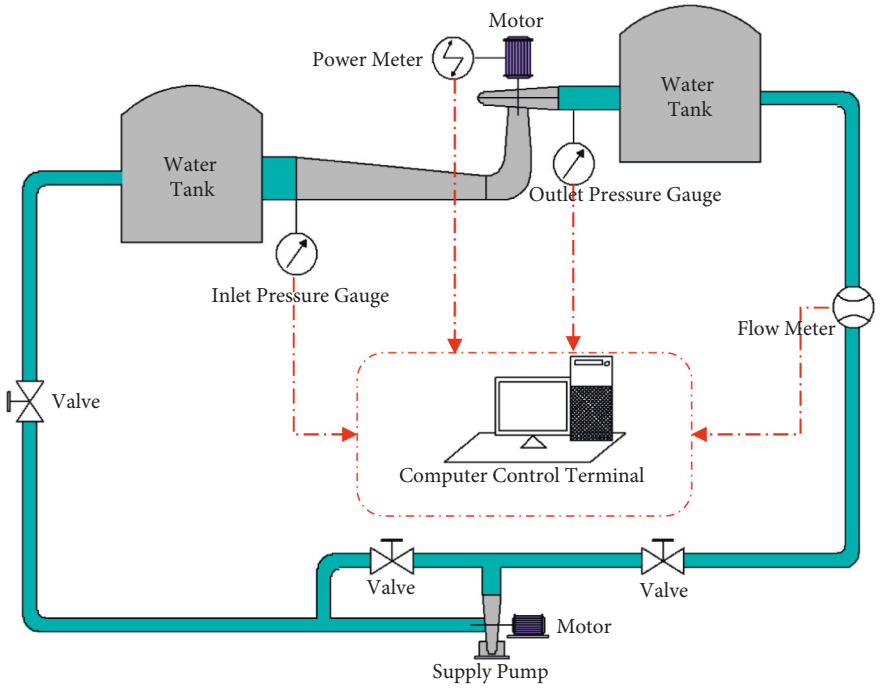

Figure 4: Schematic diagram of the test rig and data transmission system.

$$H = \frac{p_2 - p_1}{\rho g}, \tag{11}$$

where p_1 represents the measurement pressure value in the inlet and p_2 represents the measurement pressure in the outlet. Similarly, efficiency η is calculated by

$$\eta = \frac{(p_2 - p_1)Q}{2\pi n M}, \tag{12}$$

where M is the torque of the impeller. The active power P of pump turbine in the pump mode can be calculated by equation

$$P = \frac{\rho g Q H}{1000}. \tag{13}$$

In order to ensure the accuracy of numerical simulation, the calculation formula of numerical simulation is consistent with the test settings.

5. Results and Analysis

5.1. Comparison of Performance Curves. In the pump mode of pump turbine, head and efficiency are representative

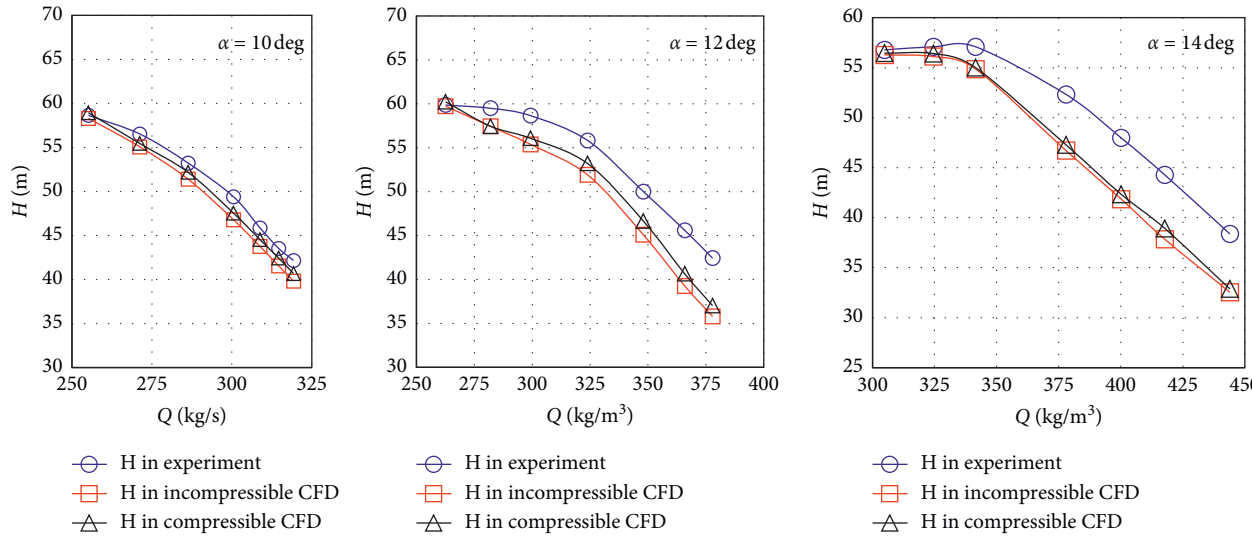

Figure 5: Comparison of head H with flow rate Q for three guide vane openings.

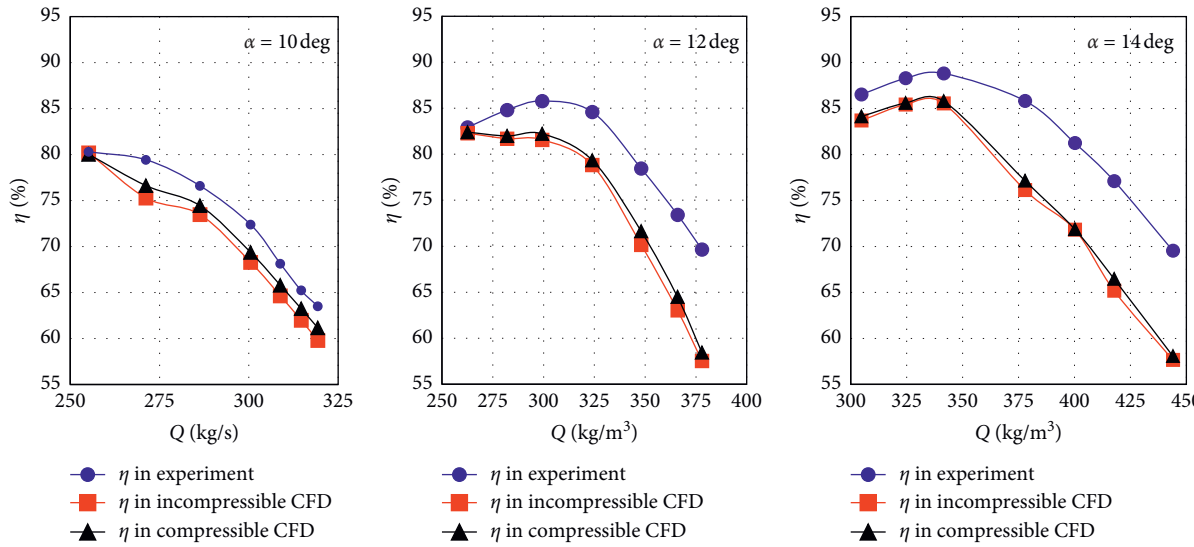

Figure 6: Comparison of efficient η with flow rate Q for three guide vane openings.

parameters of energy performance and their changes reflect the operation state of pump turbine. Here, under the three guide vane openings, taking the test value as the evaluation standard, the variation trend of various parameters under different flow conditions before and after considering the weak compressibility of fluid is compared and analyzed; three guide vane openings studied in this paper are 10 degrees, 12 degrees, and 14 degrees, respectively. Take 10 degrees as "small guide vane opening" studied in this paper, that is, when the small opening conditions described later in this article that means the guide vane opening is 10 degrees.

As shown in Figure 5, under the three guide vane openings, head H decreases with the increase of flow rate Q. Both the experimental values and the numerical simulation values before and after considering the weak compressibility of fluid meet this law; however, the curves which consider the weak compressibility of fluid are closer to the experimental values curves, and the smaller the guide vane opening is, the more obvious this phenomenon is; in other words, the influence of weak compressibility of fluid on the accuracy of head is more obvious under the condition of small guide vane opening.

Figure 6 shows the change of efficiency η with flow rate Q with different guide vane openings, which is similar to the Q-H curve. The simulated value considering the weak compressibility of fluid is closer to the experimental value, especially under the condition of small guide vane opening. The comparison of these three groups of curves shows that considering the weak compressibility of fluid can make the simulated value more accurate.

In order to further analyze the influence of weak compressibility of fluid on the performance parameters of pump turbine, the difference between the simulated value and the experimental value before and after considering the weak compressibility of fluid is analyzed; in this way, the importance of considering compressibility to the performance

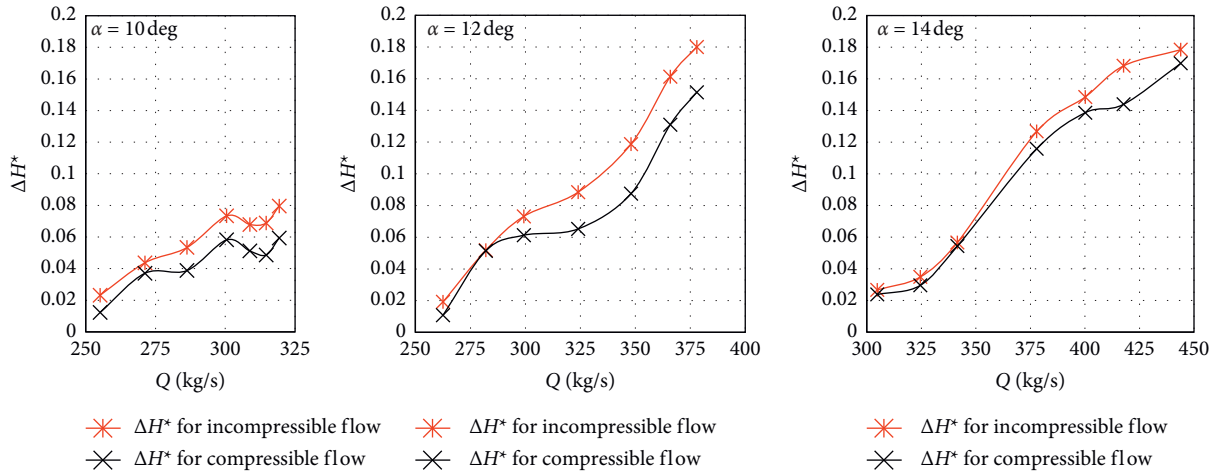

Figure 7: Comparison of ΔH^* with flow rate Q for three guide vane openings.

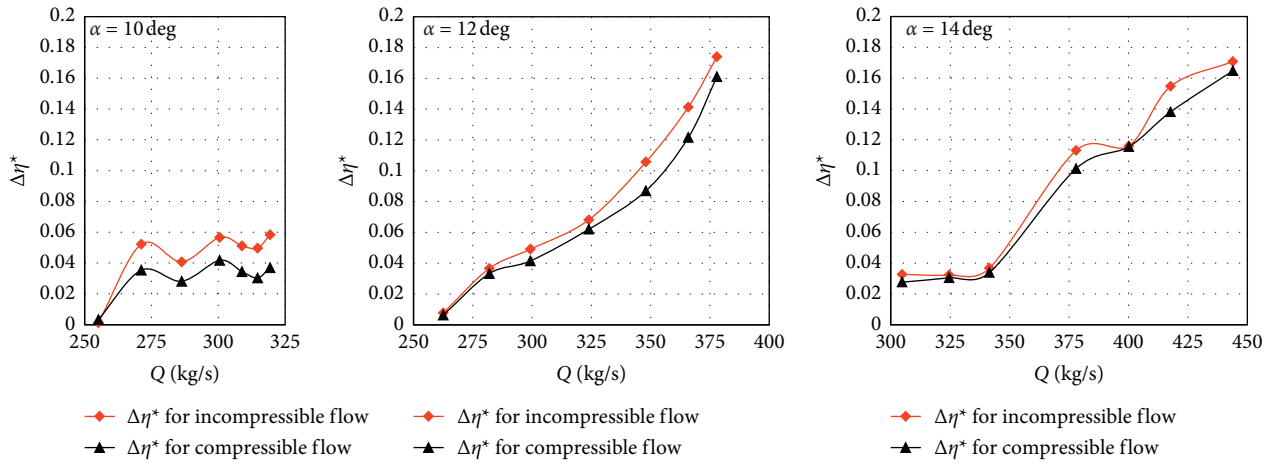

Figure 8: Comparison of $\Delta\eta^*$ with flow rate Q for three guide vane openings.

parameters of pump turbine can be seen more intuitively. Here, using equation (14) to define the head difference ΔH^* between the head numerical simulation value H_{CFD} and the head experimental value H_{EXP}, equation (15) defines the efficiency difference $\Delta\eta^*$ between numerical simulation value of efficiency η_{CFD} and efficiency experimental values η_{EXP}:

$$\Delta H^* = \left|\frac{H_{CFD} - H_{EXP}}{H_{EXP}}\right|, \tag{14}$$

$$\Delta\eta^* = \left|\frac{\eta_{CFD} - \eta_{EXP}}{\eta_{EXP}}\right|. \tag{15}$$

Figure 7 is the comparison curve of the difference between simulation value of the compressible flow or incompressible flow and the experimental value under different guide vane openings. On the whole, the head difference of compressible flow is lower than that of incompressible flow, and under the condition with small guide vane opening, the head difference is small as a whole, and it can be seen from the trend of curve that when the guide vane opening is small, which is 10 degrees, the change of head difference is relatively gentle, and with the increase of flow rate, the rise of head difference curve is relatively flat, which shows that after considering the weak compressibility of fluid; the head value of numerical simulation is closer to the experimental value, and it is most obvious when the guide vane opening is 10 degrees. As shown in Figure 8, the comparison of efficiency difference curves between compressible or incompressible flow and experiments under different openings are shown. On the whole, the efficiency difference of compressible flow is less than that of incompressible flow; when the guide vane opening α is 10 degrees, the efficiency difference does not show an upward trend, but a relatively stable fluctuation, and it shows that considering the weak compressibility of fluid, the accuracy of efficiency simulation value is improved more obviously when the guide vane opening is small.

Generally, considering the weak compressibility of the fluid, the head, efficiency, and shaft power of the pump turbine are obviously improved, and the consistency between the simulated value and the experimental value is obviously improved, while this improvement is more obvious under the condition of small guide vane opening with

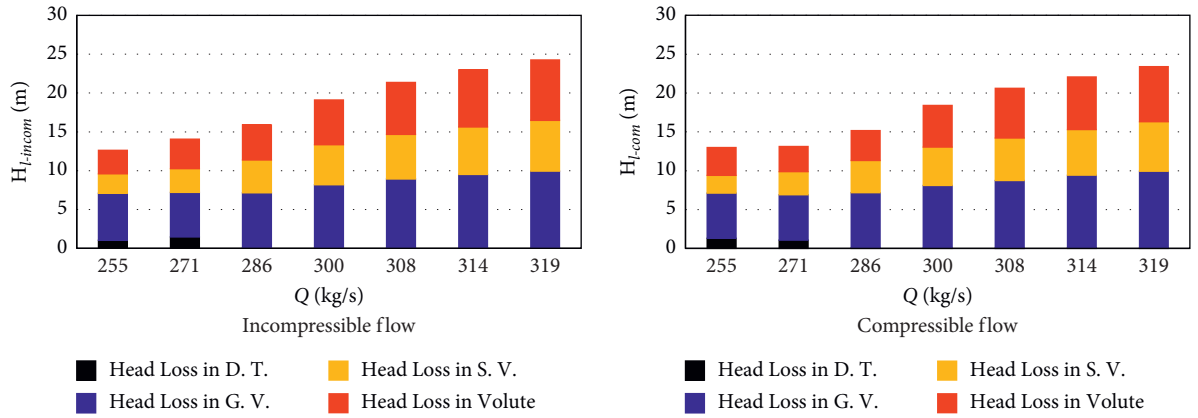

Figure 9: Stacked column chart of head loss for each component in 10-degree opening.

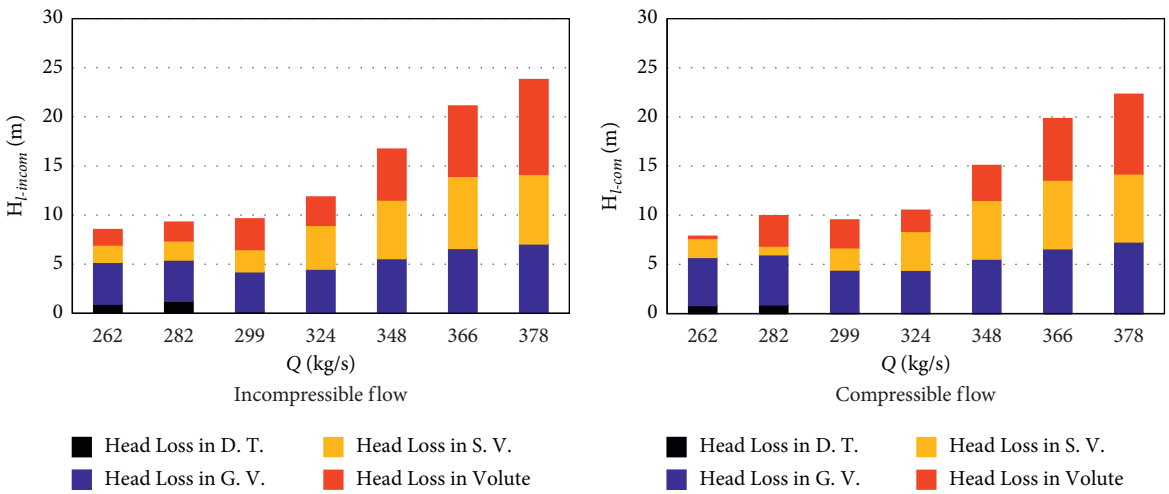

Figure 10: Stacked column chart of head loss for each component in 12-degree opening.

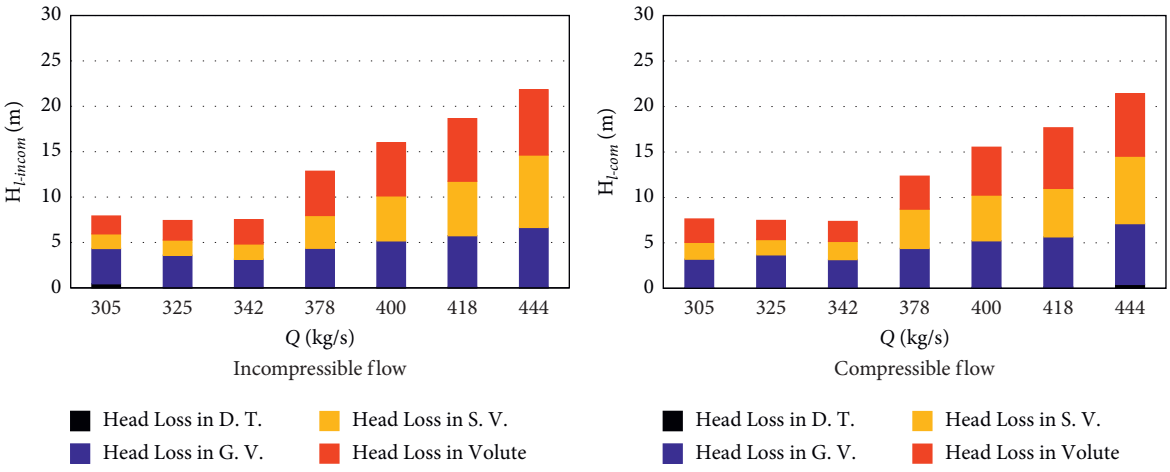

Figure 11: Stacked column chart of head loss for each component in 14-degree opening.

larger flow rate. It means that considering the weak compressibility of fluid under the condition of small guide vane opening is of great significance to improve the accuracy of numerical simulation.

5.2. Hydraulic Loss in Components. In order to further analyze the influence of weak compressibility of fluid on the performance of pump turbine, stacked column charts are made for the head loss of each component of pump turbine

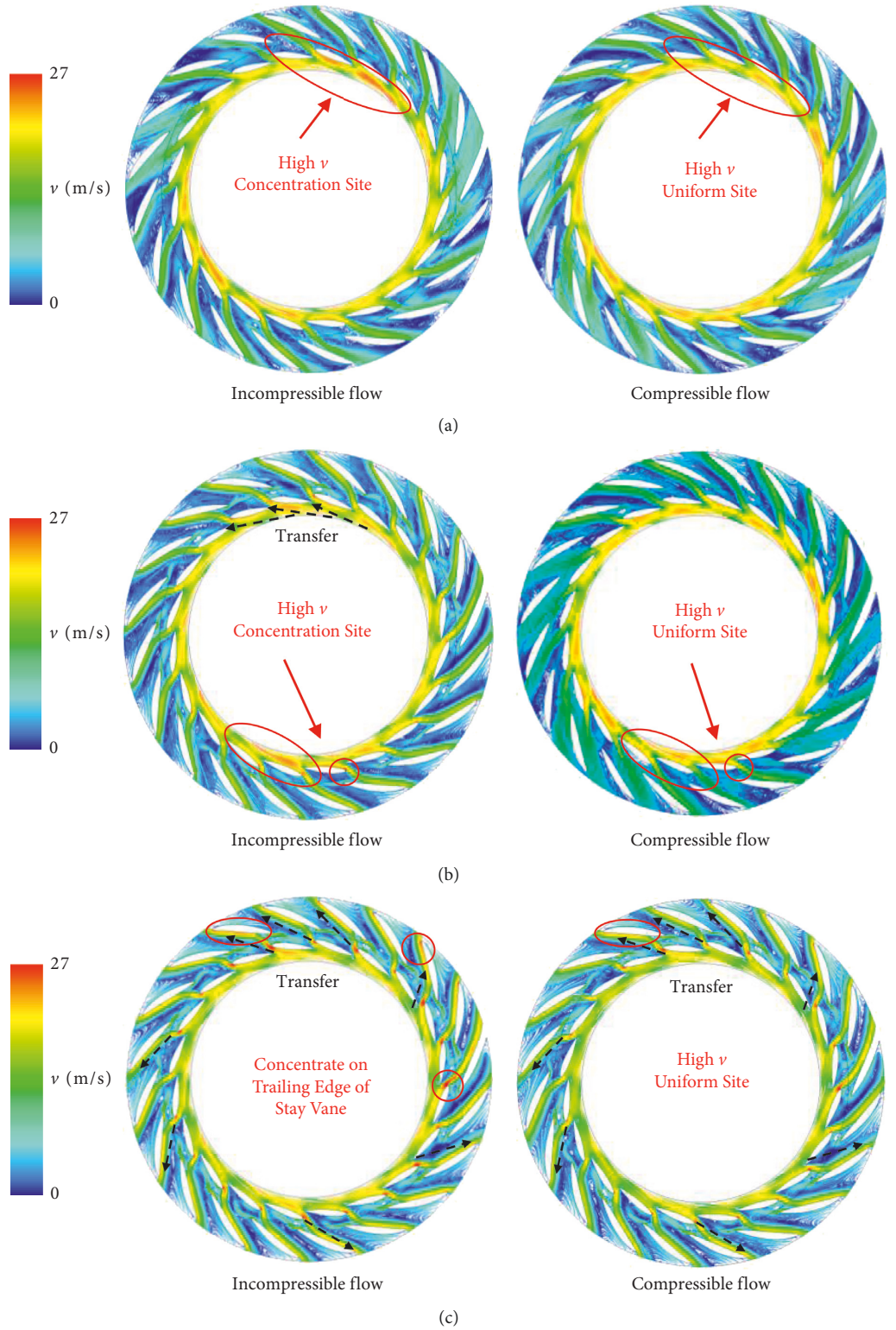

Figure 12: Velocity streamline diagrams for 10-degree guide vane opening. (a) Q = 255 kg/s, (b) Q = 286 kg/s, (c) Q = 314 kg/s.

before and after considering weak compressibility of the fluid, and then, the influence of compressibility on the head loss of each component of guide vane can be analyzed.

As shown in Figures 9–11, they are stacked column charts of the head loss of each component for compressible flow and incompressible flow in the pump turbine. It can be seen that after considering the weak compressibility of fluid, the loss of each component decreases significantly, among which the more obvious components are guide vane, stay vane, and volute. Under

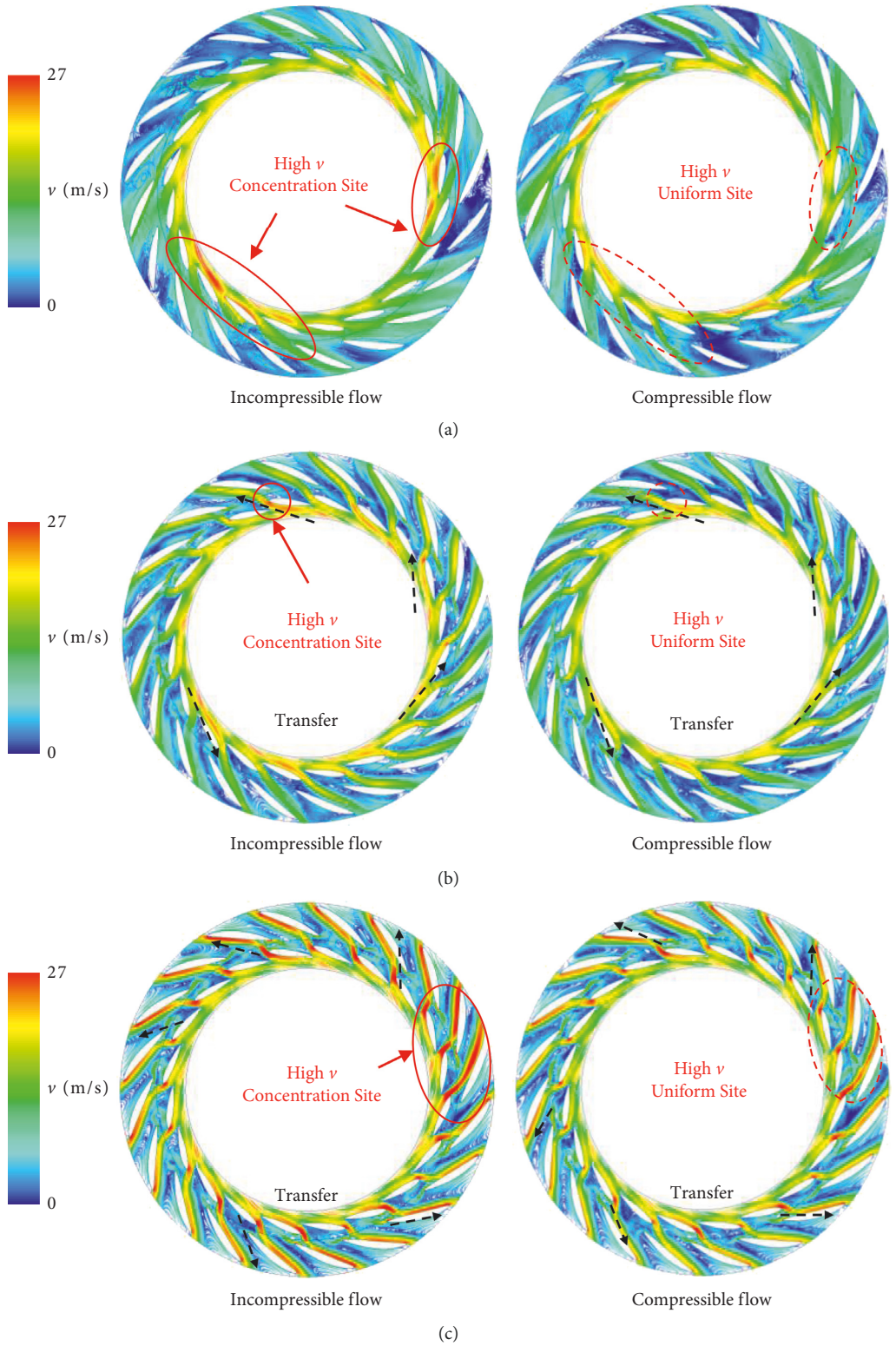

Figure 13: Velocity streamline diagrams for 12-degree guide vane opening. (a) Q = 266 kg/s, (b) Q = 324 kg/s, (c) Q = 378 kg/s.

each guide vane opening, the total loss decreases more obviously with the increase of flow rate and this phenomenon is most obvious under the condition of small guide vane opening, which also explains that in the previous section, when the guide vane opening is small, the head simulation value is in better agreement with the experimental value. In addition, comparing the head loss before and after considering the weak compressibility of fluid for each guide vane opening, the loss is the largest when the opening of the guide vane is small, but the final

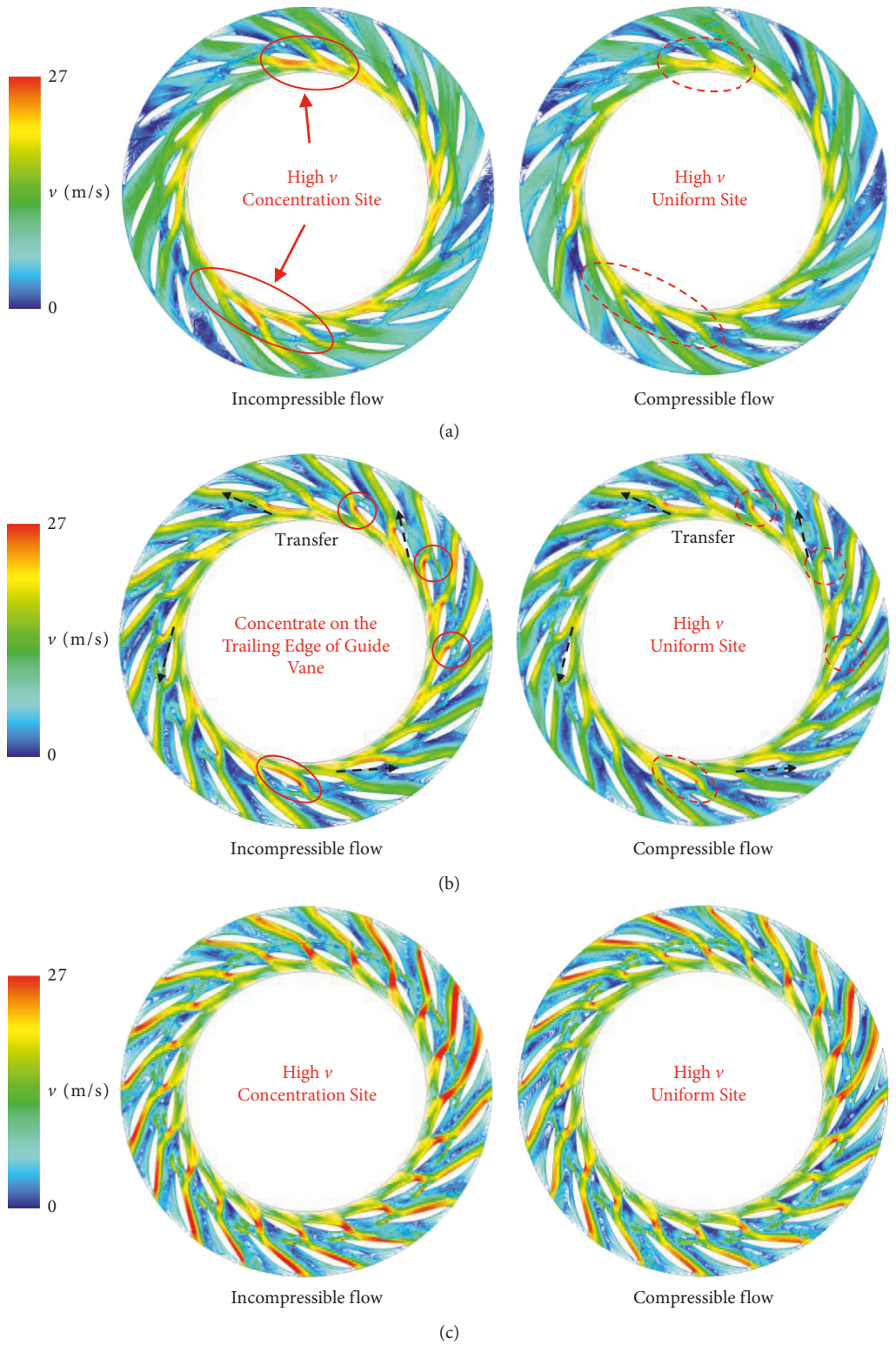

Figure 14: Velocity streamline diagrams for 14-degree guide vane opening. (a) Q = 325 kg/s, (b) Q = 378 kg/s, (c) Q = 444 kg/s.

simulated value is in the highest agreement with the experimental value; this also shows that considering the weak compressibility of fluid has the greatest impact on the accuracy of the simulation under the condition of the small guide vane opening.

5.3. Flow Patterns. Because before and after considering the weak compressibility of fluid, the reduction of head loss of pump turbine occurs mostly in the components of the guide vane and stay vane, so it is very necessary to analyze the internal flow pattern of guide vane and stay vane of pump

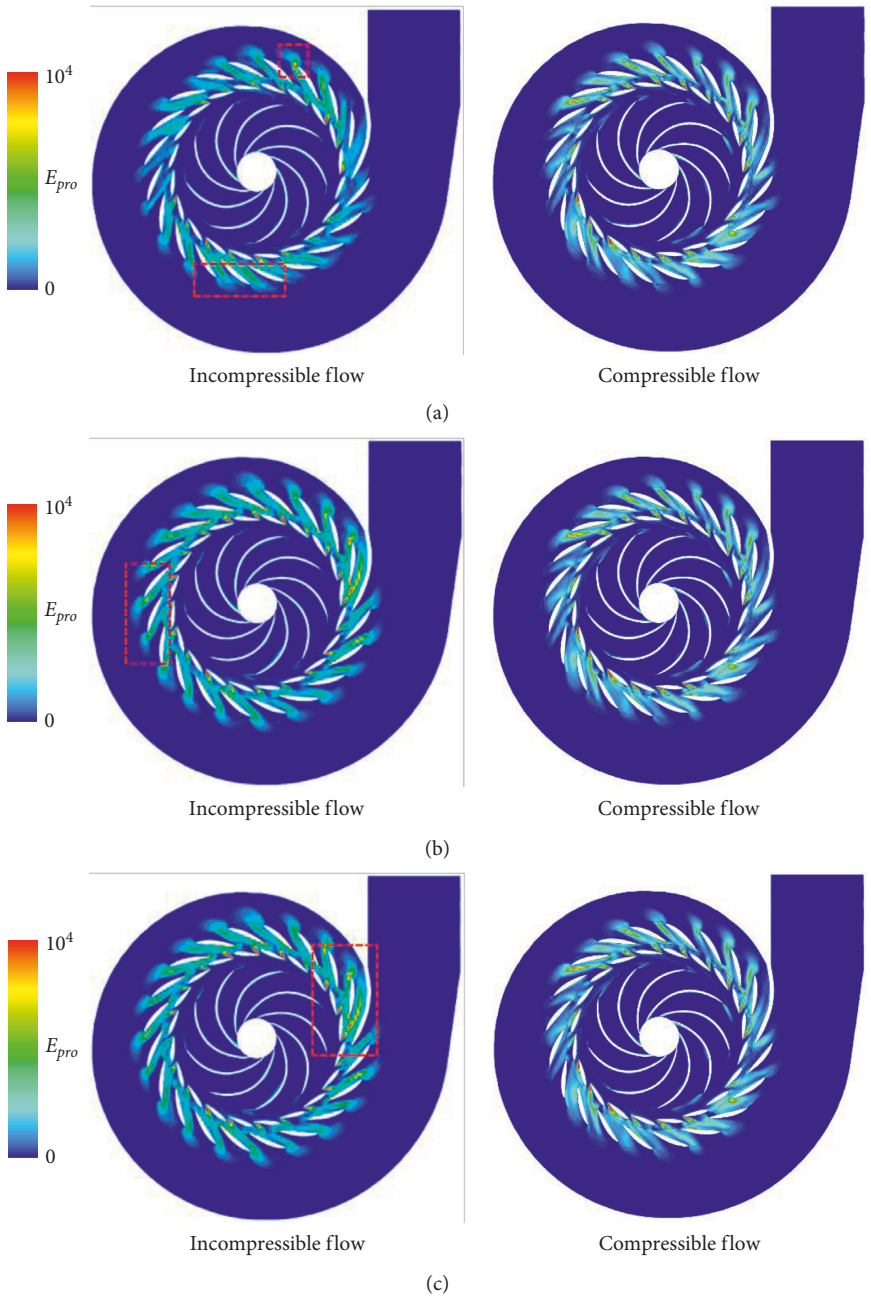

Figure 15: Contour of entropy production rate E_{pro} for 10-degree guide vane opening. (a) Q = 255 kg/s, (b) Q = 286 kg/s, (c) Q = 314 kg/s.

turbines. For the seven different flow rate working conditions studied in this research, this section will analyze three typical flow rate working conditions for each guide vane opening.

As shown in Figure 12, it is velocity stream diagrams when guide vane opening is 10 degrees. It can be seen that in the incompressible flow, the velocity distribution is obvious uneven; under the condition of small guide vane opening, with the increase of flow rate, the high-velocity site is gradually concentrated at the leading edge of guide vane blades; with the further increase of flow rate, the high-velocity site is gradually transferred from the guide vane to the channel of stay vane. However, this phenomenon has been significantly improved after considering the weak compressibility of fluid. It shows that considering the weak compressibility of fluid can improve the uniformity of velocity inside the components and improve the degree of flow disorder inside the components to a certain extent; thus, the kinetic energy loss inside the pump turbine is reduced, so as to significantly improve the performance of the pump turbine.

Shown in Figures 13and 14 are velocity streamline diagrams when guide vane opening is 12 degrees and 14 degrees, respectively; it is basically consistent with the situation when the guide vane opening is 10 degrees; that is, with the increase of flow rate, the uneven high-velocity site is concentrated from vaneless space to the trailing edge of guide vane blades; then, the uneven high-velocity site

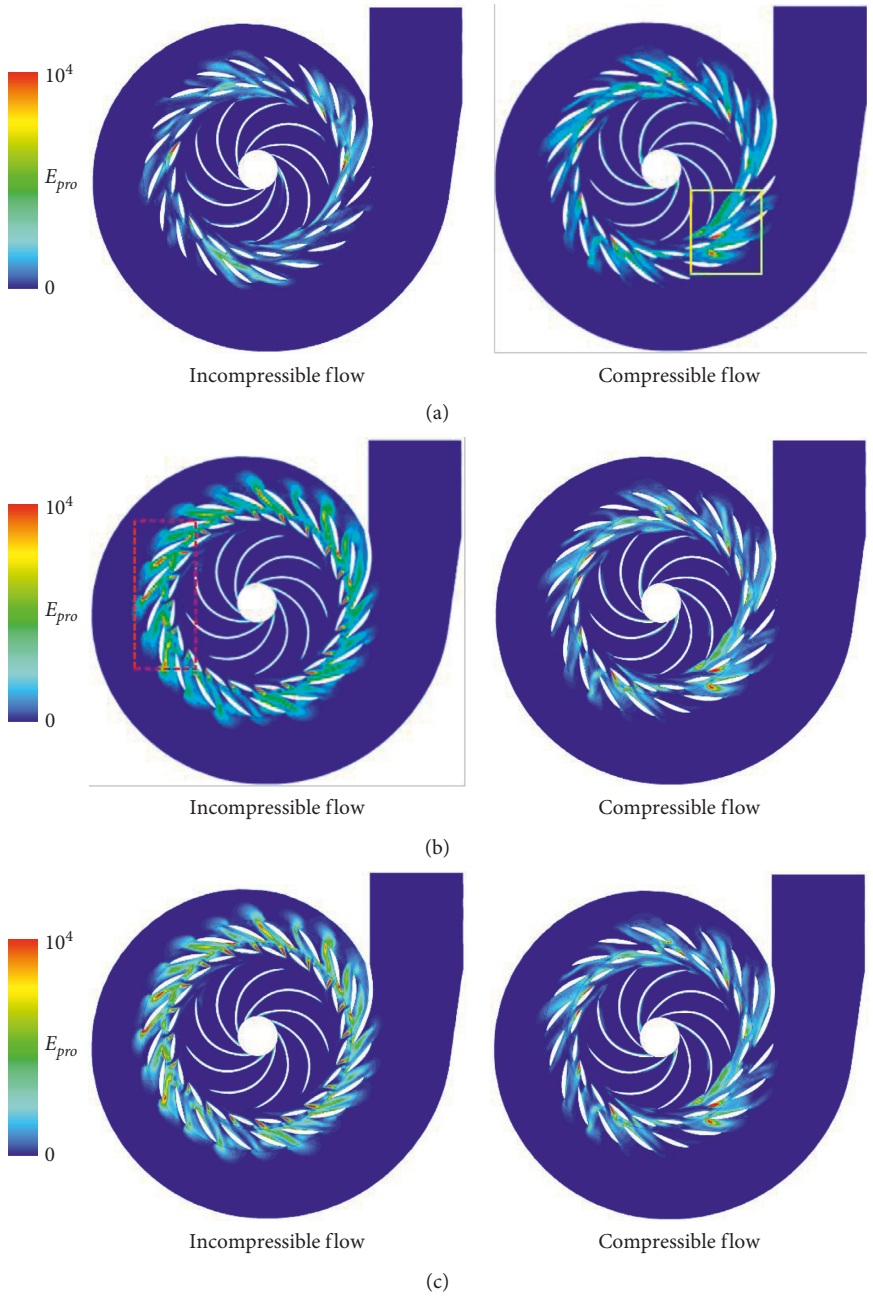

Figure 16: Contour of entropy production rate E_{pro} for 12-degree guide vane opening. (a) Q = 266 kg/s, (b) Q = 324 kg/s, (c) Q = 378 kg/s.

transferred to the channel of stay vane. The difference is that with the increase of guide vane opening, the phenomenon of uneven high-velocity site transferring from guide vane to the stay vane is more obvious.

That is to say, under the condition of small guide vane opening, considering the weak compressibility of fluid, what improves more is the uniformity of the velocity inside the guide vane blade and the disturbance of the flow. For the condition of larger guide vane opening, considering the weak compressibility of fluid, what improves more is the uniformity of the velocity inside the vane blade channels. It reduces the difference between numerical simulation results and experimental results.

5.4. Flow Energy Loss. Entropy production rate E_{pro} is usually used to evaluate the flow energy loss inside pump turbine [30, 31]. The larger the value, the greater the energy loss. Its definition is

$$E_{\text{pro}} = \frac{\beta\rho\omega k}{T}, \tag{16}$$

where β is the model closure constant, given $\beta = 0.09$, ω is the turbulent eddy frequency, k is the turbulent energy, ρ is the fluid density, and T is the temperature of 20°C.

As shown in Figures 15–17, for the contour of entropy production rate under different conditions with three guide blade openings, it can be seen that the entropy production

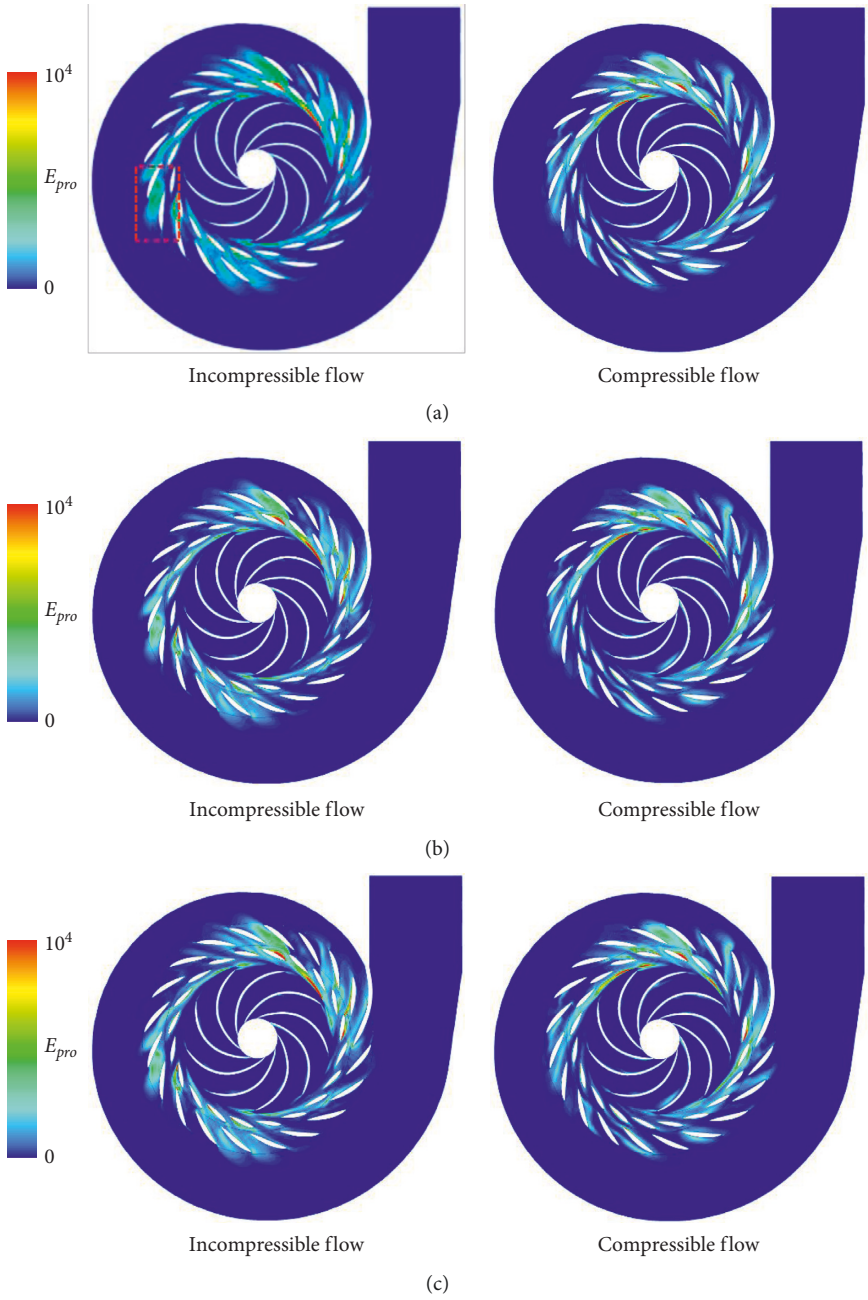

Figure 17: Contour of entropy production rate E_{pro} for 14-degree guide vane opening. (a) Q = 325 kg/s, (b) Q = 378 kg/s, (c) Q = 444 kg/s.

rate decreases after considering the weak compressibility of fluid, which is still most obvious under the small guide vane opening. As shown in Figure 15, in incompressible flow with guide vane opening of 10 degrees, the entropy production rate is highly concentrated in the leading edge of the guide vane blade. At the guide vane opening of 10 degrees, with the increase of flow rate, the entropy production rate at the stay vane near the cut water increases gradually; however, these losses are improved in the flow which considers the weak compressibility of fluid.

As shown in Figure 16, when the opening of guide vane is 12 degrees, there is a large loss of stay vane and guide vane in compressible flow under the condition of small flow rate, which may be due to the low matching degree between guide vane opening and flow rate, resulting in the vortex in the channel and large energy loss. Nevertheless, with the increase of flow rate, the loss in incompressible flow increases, mainly in the guide vane and stay vane; there is also some small increase in the volute, but in the flow considering the weak compressibility of fluid, the energy change is still relatively stable without obvious increase; it also shows that considering the weak compressibility of fluid, the whole flow energy loss is reduced and the stability of internal entropy production rate is maintained.

As shown in Figure 17, when the opening of the guide vane is 14 degrees, the energy loss in the incompressible flow

is mainly concentrated on the stay vane; after considering the weak compressibility of fluid, the energy loss improves most obvious where is the component of stay vane, especially the energy loss near the cut water.

Generally, with the increase of guide vane opening, the energy loss is large in the components which are transferred from the leading edge of guide vane to the trailing edge of the stay vane. Moreover, considering the weak compressibility of fluid, the energy loss is obviously improved under all three guide vane openings. At the same time, considering the weak compressibility of fluid has the ability to reduce the predicted local high energy loss. With the increase of flow rate, the energy loss of incompressible flow increases under different guide vane openings, while the energy loss of compressible flow is almost unchanged. This is why the compressible case has the predicted hydrodynamic performance closer to the experimental value.

6. Conclusions

Based on the model test results and the comparative numerical simulations, the influence of weak compressibility on predicting the hydrodynamic performance of pump turbine is studied in detail. Conclusions can be drawn as follows:

(1) In the prediction of head H and efficiency η, considering the weak compressibility of fluid will make simulation results closer to experimental results. The improvement is more obvious when guide vane opening is smaller but the flow rate is larger. This is because that the smaller the guide vane opening, the more serious the channel blockage, which leads to more pressurized flow from runner. Hence, it is of great significance to consider the weak compressibility of fluid when the guide vane opening is small.

(2) The difference between compressible flow field and incompressible flow field is found mainly because of the guide vane blockage. However, with the increase of guide vane opening or flow rate, the influence will extend to all the downstream components including guide vane, stay vane, and volute. This phenomenon shows that the influence of fluid weak compressibility is continuous, cumulative, and necessary to consider. It also shows that considering the weak compressibility of the fluid is of great significance to improve the flow pattern of the whole channel.

(3) Considering the weak compressibility of fluid can change the prediction of pressure, velocity, and other fields in simulation. Especially in the case of serious flow blockage, considering the weak compressibility of fluid is more important to the accuracy of prediction field. When simulating the compressible flow field, velocity and pressure distribution are more uniform. With a more uniform distribution of pulsating velocity, the prediction of local very strong entropy production is avoided, while the difference between numerical and experimental results is reduced.

Generally, it is necessary to simulate the weakly compressible flow especially when the pump turbine operates in small guide vane opening condition. In the investigation of reversible pump turbine operating in off-design conditions and condition conversion processes, the weak compressibility is required in flow simulations.

Data Availability

The data used to support the findings of this study are available from the corresponding author upon request.

Conflicts of Interest

The authors declare that they have no conflicts of interest.

Acknowledgments

The authors would like to acknowledge the financial support of National Natural Science Foundation of China, under grant number 51909131.

References

[1] Y. Zhang, X. Zheng, J. Li, and X. Du, "Experimental study on the vibrational performance and its physical origins of a prototype reversible pump turbine in the pumped hydro energy storage power station," *Renewable Energy*, vol. 130, pp. 667–676, 2019.

[2] J. Xu and T. Liu, "Optimal hourly scheduling for wind–hydropower systems with integrated pumped-storage technology," *Journal of Energy Engineering*, vol. 147, no. 3, 2021.

[3] K. Liu, J. He, Z. Luo et al., "Load frequency control of pumped storage power station based on LADRC," *Processes*, vol. 8, p. 380, 2020.

[4] B. Wang, T. Ruan, Y. Chen et al., "Graphene-based composites for electrochemical energy storage," *Energy Storage Materials*, vol. 24, pp. 22–51, 2020.

[5] S. Ould Amrouche, D. Rekioua, T. Rekioua, and S. Bacha, "Overview of energy storage in renewable energy systems," *International Journal of Hydrogen Energy*, vol. 41, pp. 20914–20927, 2016.

[6] M. Mahmoud, M. Ramadan, A. G. Olabi, K. Pullen, and S. Naher, "A review of mechanical energy storage systems combined with wind and solar applications," *Energy Conversion and Management*, vol. 210, Article ID 112670, 2020.

[7] T. Ma, H. Yang, L. Lu, and J. Peng, "Pumped storage-based standalone photovoltaic power generation system: Modeling and techno-economic optimization," *Applied Energy*, vol. 137, pp. 649–659, 2015.

[8] M. Vitek, T. Kralik, and J. Tuma, *The Role of Pumped Storage Power Plants in the Power System Operation*, pp. 1–5, IEEE, Piscataway, NJ, USA, 2016.

[9] M. S. Javed, T. Ma, J. Jurasz, and M. Y. Amin, "Solar and wind power generation systems with pumped hydro storage: Review and future perspectives," *Renewable Energy*, vol. 148, pp. 176–192, 2020.

[10] S. Rehman, L. M. Al-Hadhrami, and M. M. Alam, "Pumped hydro energy storage system: A technological review," *Renewable and Sustainable Energy Reviews*, vol. 44, pp. 586–598, 2015.

[11] D. Connolly, H. Lund, P. Finn, B. V. Mathiesen, and M. Leahy, "Practical operation strategies for pumped hydroelectric energy storage (PHES) utilising electricity price arbitrage," *Energy Policy*, vol. 39, pp. 4189–4196, 2011.

[12] D. Y. Li, L. Han, H. J. Wang, R. Z. Gong, X. Z. Wei, and D. Q. Qin, "Flow characteristics prediction in pump mode of a pump turbine using large eddy simulation," *Proceedings of the Institution of Mechanical Engineers—Part E: Journal of Process Mechanical Engineering*, vol. 231, pp. 961–977, 2017.

[13] R. Tao and Z. Wang, "Comparative numerical studies for the flow energy dissipation features in a pump-turbine in pump mode and turbine mode," *Journal of Energy Storage*, vol. 41, Article ID 102835, 2021.

[14] X. Su, S. Huang, X. Zhang, and S. Yang, "Numerical research on unsteady flow rate characteristics of pump as turbine," *Renewable Energy*, vol. 94, pp. 488–495, 2016.

[15] Z. Li, H. Bi, B. Karney, Z. Wang, and Z. Yao, "Three-dimensional transient simulation of a prototype pump-turbine during normal turbine shutdown," *Journal of Hydraulic Research*, vol. 55, pp. 520–537, 2017.

[16] Y. C. Li, C. M. Cheng, Y. L. Lo, F. M. Fang, and D. Q. Zheng, "Simulation of turbulent flows around a prism in suburban terrain inflow based on random flow generation method simulation," *Journal of Wind Engineering and Industrial Aerodynamics*, vol. 146, pp. 51–58, 2015.

[17] G. N. Lygidakis and I. K. Nikolos, "Numerical analysis of flow over the NASA common research model using the academic computational fluid dynamics code galatea," *Journal of Fluids Engineering*, vol. 137, no. 7, 2015.

[18] J. A. Heyns, A. G. Malan, T. M. Harms, and O. F. Oxtoby, "A weakly compressible free-surface flow solver for liquid–gas systems using the volume-of-fluid approach," *Journal of Computational Physics*, vol. 240, pp. 145–157, 2013.

[19] K. Ardalan, D. I. Meiron, and D. I. Pullin, "Steady compressible vortex flows: The hollow-core vortex array," *Journal of Fluid Mechanics*, vol. 301, pp. 1–17, 1995.

[20] V. Daru, P. Le Quéré, M. C. Duluc, and O. Le Maître, "A numerical method for the simulation of low Mach number liquid–gas flows," *Journal of Computational Physics*, vol. 229, pp. 8844–8867, 2010.

[21] I. J. Keshtiban, F. Belblidia, and M. F. Webster, "Numerical simulation of compressible viscoelastic liquids," *Journal of Non-Newtonian Fluid Mechanics*, vol. 122, pp. 131–146, 2004.

[22] C. C. S. Song and M. Yuan, "A weakly compressible flow model and rapid convergence methods," *Journal of Fluids Engineering*, vol. 110, pp. 441–445, 1988.

[23] N. M. C. Martins, A. K. Soares, H. M. Ramos, and D. I. C. Covas, "CFD modeling of transient flow in pressurized pipes," *Computers & Fluids*, vol. 126, pp. 129–140, 2016.

[24] G. Wu, X. Duan, J. Zhu, X. Li, X. Tang, and H. Gao, "Investigations of hydraulic transient flows in pressurized pipeline based on 1D traditional and 3D weakly compressible models," *Journal of Hydroinformatics*, vol. 23, pp. 231–248, 2021.

[25] X. Tang, X. Duan, H. Gao, X. Li, and X. Shi, "CFD investigations of transient cavitation flows in pipeline based on weakly-compressible model," *Water*, vol. 12, p. 448, 2020.

[26] F. R. Menter, M. Kuntz, and R. Langtry, "Ten years of industrial experience with the SST turbulence model," *Turbulence Heat and Mass Transfer*, vol. 4, pp. 625–632, 2003.

[27] D. Li, H. Wang, G. Xiang, R. Gong, X. Wei, and L. Zhansheng, "Unsteady simulation and analysis for hump characteristics of a pump turbine model," *Renewable Energy*, vol. 77, pp. 32–42, 2015.

[28] I. B. Celik, U. Ghia, P. J. Roache, and C. J. Freitas, "Procedure for estimation and reporting of uncertainty due to discretization in CFD applications," *Journal of Fluids Engineering-Transactions of the ASME*, vol. 130, no. 7, 2008.

[29] IEC Standards, *Hydraulic Turbines, Storage Pumps And Pump-Turbines-Model Acceptance Tests*, IEC, Lausanne, Switzerland, 1999.

[30] F. Kock and H. Herwig, "Local entropy production in turbulent shear flows: a high-Reynolds number model with wall functions," *International Journal of Heat and Mass Transfer*, vol. 47, pp. 2205–2215, 2004.

[31] Q. Zhou, L. Xia, and C. Zhang, "Internal mechanism and improvement criteria for the runaway oscillation stability of a pump-turbine," *Applied Sciences*, vol. 8, no. 11, p. 2193, 2018.